Role of Columnar Mesophase in the Morphological Evolution of Polymer Single Crystals upon Heating: A Combined Atomic Force Microscopy and Electron Diffraction Study

Raluca I. Gearba,[†,‡] Nicolas Dubreuil,[†] Denis V. Anokhin,[†,‡] Yuli K. Godovsky,[§,||] Jr-Jeng Ruan,[⊥] Annette Thierry,[⊥] Bernard Lotz,[⊥] and Dimitri A. Ivanov*[,†,‡]

Laboratoire de Physique des Polymères, CP-223, Université Libre de Bruxelles, Boulevard du Triomphe, B-1050, Brussels, Belgium, Karpov Institute of Physical Chemistry, 10 Vorontsovo Pole, 103064 Moscow, Russia, and Institut Charles Sadron, 6 Rue Boussingault, Strasbourg 67083, France

Received July 22, 2005; Revised Manuscript Received October 19, 2005

ABSTRACT: The crystal-to-hexagonal columnar mesophase transition in solution-grown single crystals of poly(di-*n*-propyl siloxane), PDPS, was studied in situ with selected-area electron diffraction and variable-temperature atomic force microscopy. It was observed that, upon the transition, the hexagonal columnar mesophase displays two mutually orthogonal orientations of the lattice. The 2**a*** and 2**b*** reciprocal lattice vectors of the α-phase crystal coincide with the **a*** vectors of each of the two differently oriented mesophase lattices. The in situ atomic force microscopy study of the evolution of a single PDPS crystal upon heating shows that crystal thickening can occur via a short-term dwelling in the mesophase. The high chain mobility in the mesophase can account for the exceptional range of accessible crystal thicknesses of PDPS, which is much larger than that observed for polyethylene single crystals.

I. Introduction

The mechanisms of polymer chain folding during crystallization and the structure of the resulting crystal/amorphous interface has been the focus of numerous studies since the discovery of folded-chain crystals.[1] The chain unfolding and refolding mechanisms have been extensively studied on polyethylene, PE, and various model PE-like systems such as ultralong *n*-alkanes, where effects of polydispersity and structural defects are excluded.[2,3] The evolution of the crystal thickness during thermal treatments has been interpreted in terms of different mechanisms of chain unfolding[4] such as solid-state and liquid-state transformations. It was suggested[4] that, depending on the annealing versus crystallization temperatures, crystal thickening could occur either in the solid state or via a short transit through the melt. A solid-state transformation implies a certain chain mobility in the crystalline phase (the so-called α_c relaxation), which is, in some respects, analogous to rotator phases reported for short *n*-alkanes.[5] However, for the majority of conventional polymers, such as PE, the unfolding mechanism is not easily studied experimentally because the temperature interval of crystal thickening is quite narrow and the range of accessible crystal thicknesses is limited.[6] A thorough study[7] shows that melting of 1,4-*trans*-polybutadiene (PBD) occurs by transit through a columnar hexagonal mesophase that is stable over more than 55 °C. Extensive thickening of PBD single-crystal mats during annealing was studied with time-resolved X-ray diffraction. It was estimated that the crystals could thicken by several hundreds of angstroms when annealed above the crystal−mesophase transition.[7]

In the present paper, we report the first studies of crystal thickening in poly(di-*n*-propylsiloxane), PDPS, where there is a large range of accessible crystal thicknesses, as both folded and extended-chain crystals can form under ambient conditions.[8,9] PDPS exhibits two crystalline modifications, denoted α and β,[10−17] and a mesophase for which hexagonal columnar packing of the chains was suggested.[16,18] Recently, the structures of the α polymorph and the mesophase were revised.[9] It was found that the unit cell of the α phase is pseudotetragonal and is characterized by the monoclinic space group *C*2/*c* (No. 15). The lattice parameters are $a = b = 19.15$ Å and $c = 5.00$ Å. Upon cooling, the α polymorph transforms into the monoclinic β at about −46 °C, whereas it melts at approximately 62 °C. The sample clears at 197 °C by passing through a columnar hexagonal mesophase that is stable over more than 130 °C. It is generally accepted[19] that the combination of a polar backbone and apolar lateral chains is responsible for the exceptional stability of the PDPS mesophase even in the absence of any mesogenic groups in its chemical structure. In the mesophase, the PDPS chains are supposed to have a nearly extended conformation,[18] which accounts for the crystallization resulting in chain-extended crystals. It should be stressed that the formation of extended-chain polymer crystals is a rare feature, which has been mainly studied for HDPE.[20,21] However, when crystallized from solution (i.e., a fully disordered state), PDPS follows the classical crystallization route, resulting in the formation of folded-chain crystals.[8]

The present paper focuses on a study of the influence of the columnar mesophase on the thermal behavior and structural evolution of solution-grown single crystals of PDPS. The melting of PDPS single crystals was studied in real time with variable-temperature atomic force microscopy (AFM). The crystallographic relationships between the α crystalline phase and the mesophase during melting are examined with selected-area electron diffraction (ED). The question of whether crystal thickening implies a passage through a metastable state (mesophase) or happens via a solid-state transition, i.e., in the crystalline phase, is specifically addressed.

* To whom correspondence should be addressed. E-mail: dimitri.ivanov@uha.fr.
[†] Université Libre de Bruxelles.
[‡] Present address: Institut de Chimie des Surfaces et Interfaces (ICSI), UPR CNRS 9069 15 rue Jean Starcky, B. P. 2488, 68057 Mulhouse Cedex, France.
[§] Karpov Institute of Physical Chemistry.
[||] Unexpectedly passed away on May 23, 2005.
[⊥] Institut Charles Sadron.

10.1021/ma051606g CCC: $33.50
Published on Web 11/23/2005

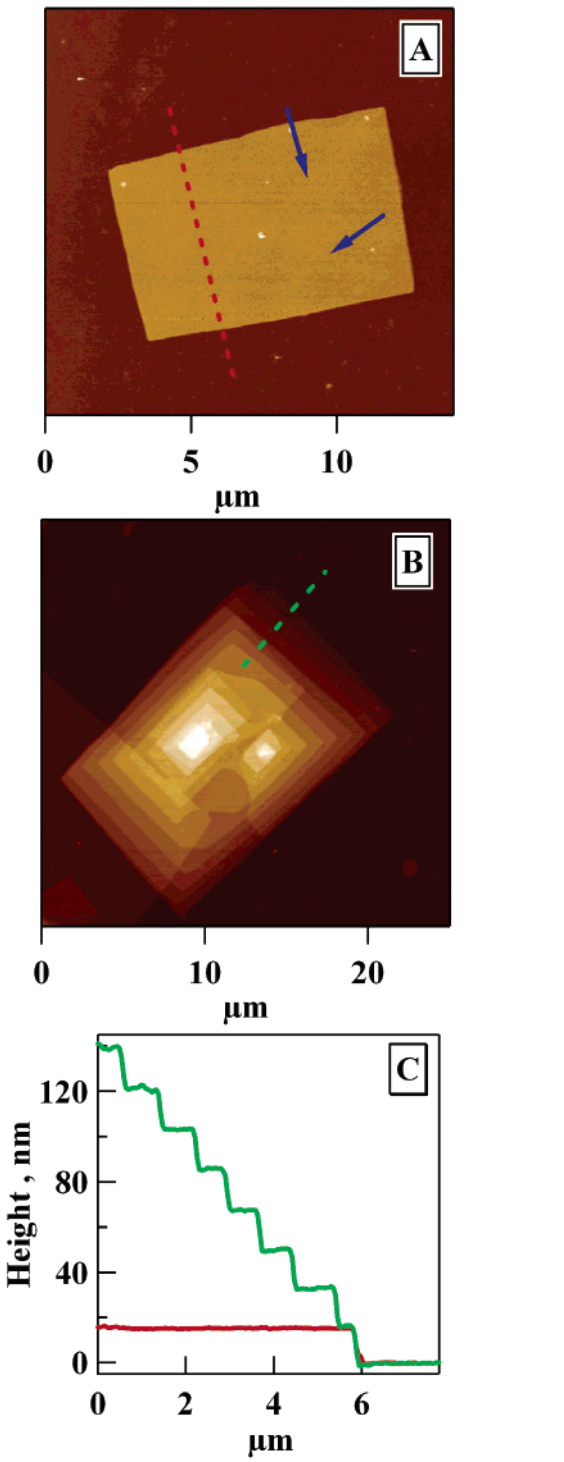

Figure 1. Tapping mode AFM images showing PDPS solution-grown single crystals. (A) Individual and (B) multilayer crystals with spiral growth. The sector boundaries in A are indicated by blue arrows. (C) Cross-section profiles measured along the red and green dashed lines show that the thickness of an individual lamella is approximately 16 nm for both crystals.

II. Materials and Methods

II.1. Materials and Sample Preparation. The PDPS sample used in this study has a molecular weight of $M_w = 87\,000$. The corresponding degree of polymerization is 670. Single crystals of PDPS were prepared by slow cooling of a 0.05% solution in *n*-butyl acetate,[8] followed by drying for several hours at the crystallization temperature. The samples were deposited on 100 μm carbon-coated mesh grids for ED measurements and on freshly cleaned Si substrates for AFM imaging.

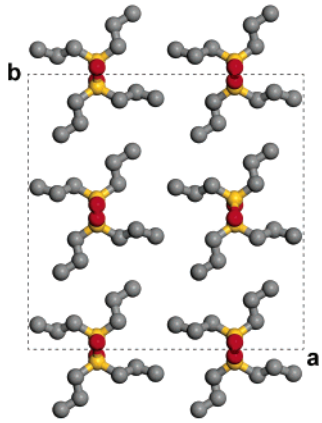

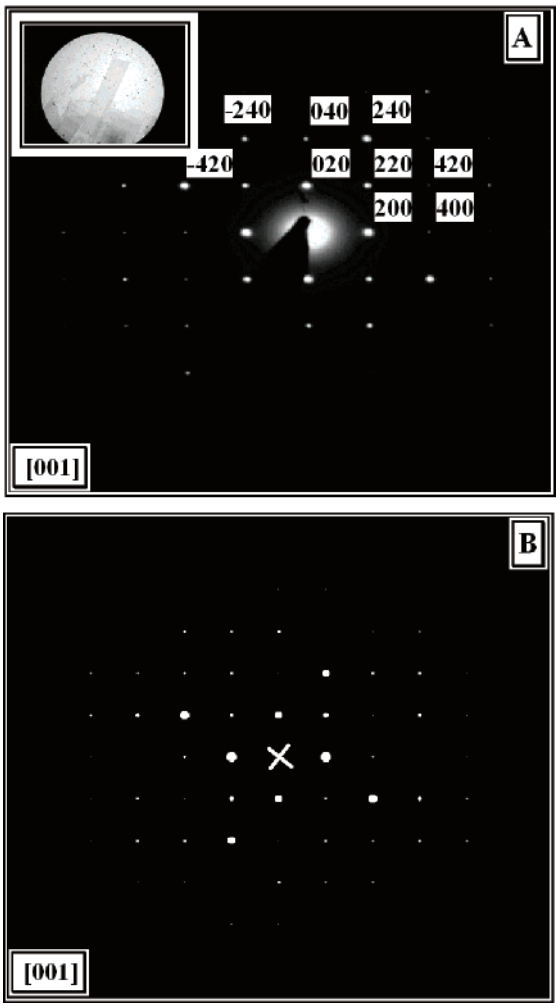

Figure 2. (A) Electron diffraction pattern corresponding to the [001] diffraction zone of a PDPS single crystal. The bright-field image of the PDPS single crystal is given in the inset. (B) Simulated electron diffraction pattern calculated for the unit cell of the α phase of PDPS proposed earlier.[9] The *ab* projection of the unit cell is shown at the top of the figure.

II.2. Electron Diffraction. Electron microscopy experiments were performed with a Phillips CM12 electron microscope operated at 120 kV with a lanthanum hexaboride (LaB_6) filament. The microscope was equipped with a tilting stage, allowing different diffraction zones to be explored.

II.3. Calculation of Electron Diffraction Patterns and Autocorrelation Functions. Electron diffraction patterns were computed

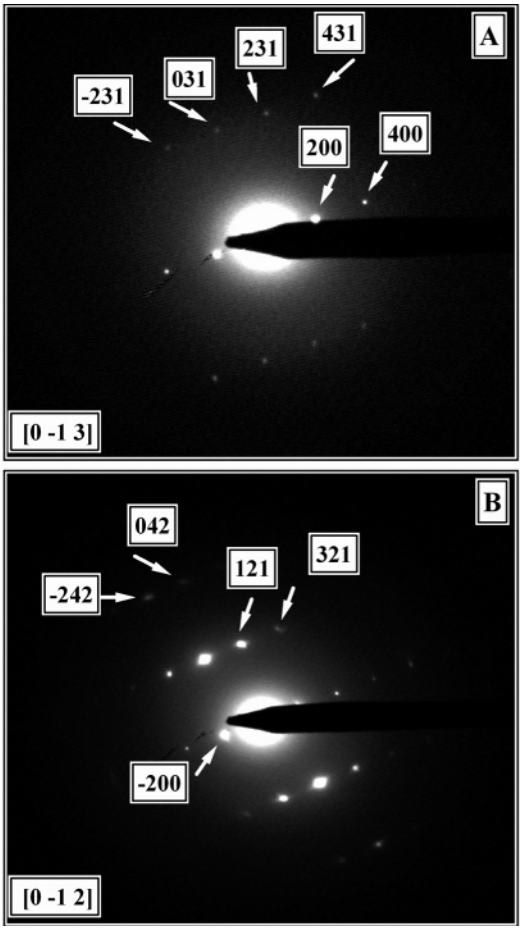

Figure 3. Diffraction patterns corresponding to the (A) [0$\bar{1}$3] and (B) [012] zone axes. The patterns were obtained by tilting the PDPS single crystals about the [010] axis by (A) 53° and (B) 64°.

using the atomic scattering factors, f_e, given by the Mott formula[22]

$$f_e = \frac{2me^2}{h^2}(Z - f_X)/s^2 \quad (1)$$

where Z is the atomic number; s is the norm of the reciprocal space vector $\underline{s}$; h is Planck's constant; e and m are the electron charge and mass, respectively; and f_X is the X-ray atomic scattering factor. The s value is defined as $2\pi\sin(\theta)/\lambda$, where θ is the Bragg angle and λ is the wavelength. The X-ray atomic scattering factors, f_X, were calculated according to

$$f_X = \sum_{i=1}^{4} a_i \exp(-b_i s^2) + c \quad (2)$$

In eq 2, the constants a_i, b_i, and c are specific to a given atomic species.[23] To take into account the thermal motion of the atoms, the atomic scattering factors, f_e, were corrected by the overall isotropic temperature factor B as follows

$$f_{e\_cor} = f_e \exp\left[-B\frac{\sin(\theta)^2}{\lambda^2}\right] \quad (3)$$

The 2D autocorrelation, or Patterson, function, $P(\underline{u})$, of the potential map was computed from experimental ED patterns as

$$P(\underline{u}) \equiv \rho(\underline{r}) \otimes \rho(-\underline{r}) = \mathrm{Re}[\sum_i |F_i(\mathbf{s})|^2 \exp(-2\pi i \underline{s}\underline{u})] \quad (4)$$

where $\underline{u}$ and $\underline{r}$ are the 2D direct space vectors and $F_i(\underline{s})$ is the structure factor of the corresponding diffraction peak. Prior to calculations, the electron diffraction patterns were background corrected.

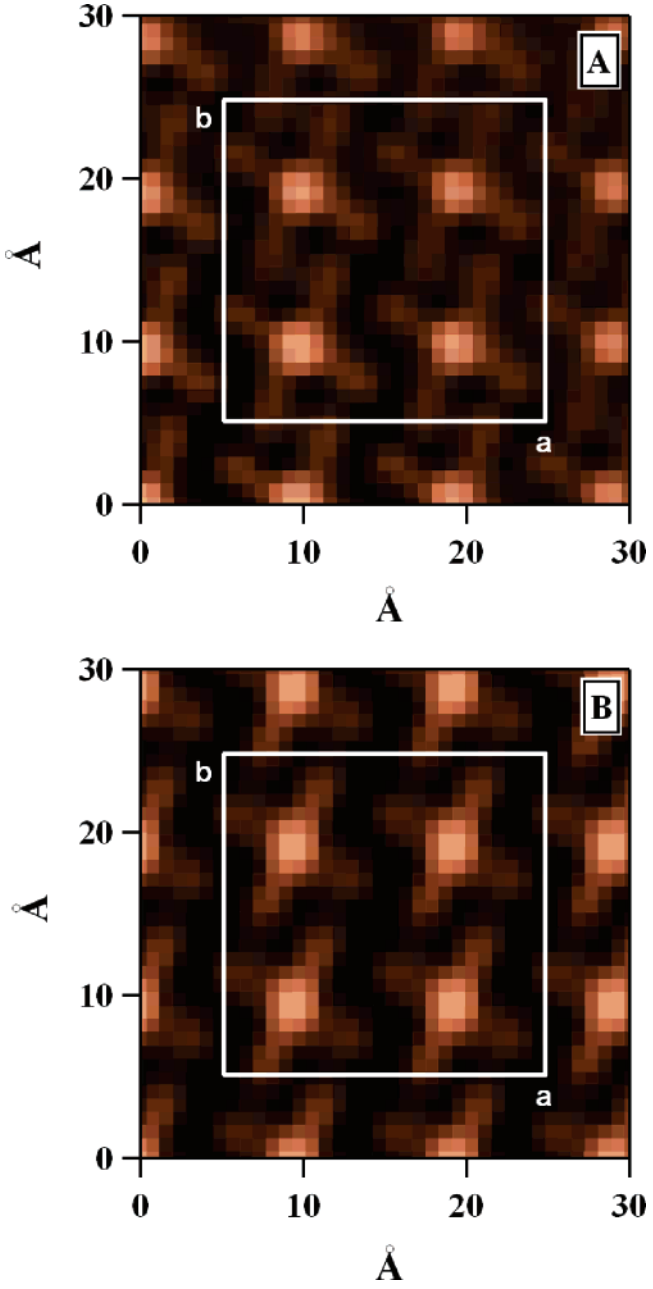

Figure 4. (A) Experimental and (B) simulated Patterson functions corresponding to the [001] diffraction zone. The white rectangle shows the unit-cell edges. The functions display the spatially localized electron-rich siloxane backbone and less-dense alkyl side chains splaying almost orthogonally.

II.4. Atomic Force Microscopy. Characterization of the crystalline morphology and thermal behavior was performed with a commercial AFM instrument (Nanoscope III, Digital Instruments/Veeco Metrology Group) equipped with a high-temperature heater accessory[24] allowing the sample and tip temperature to be varied. Briefly, the sample temperature is controlled via a thermocouple placed under the AFM pack on which the sample is mounted. The temperature of the tip is measured from its resonant frequency and can be adjusted by applying a voltage to the resistive heater placed inside the tip holder in the proximity of the piezo actuator used to drive the cantilever. More details of the AFM operation at high temperatures can be found elsewhere.[25] The vertical sensitivity of the scanner was calibrated using height standards (NT-MTD, Zelenograd, Russia) chosen according to the range of the topography

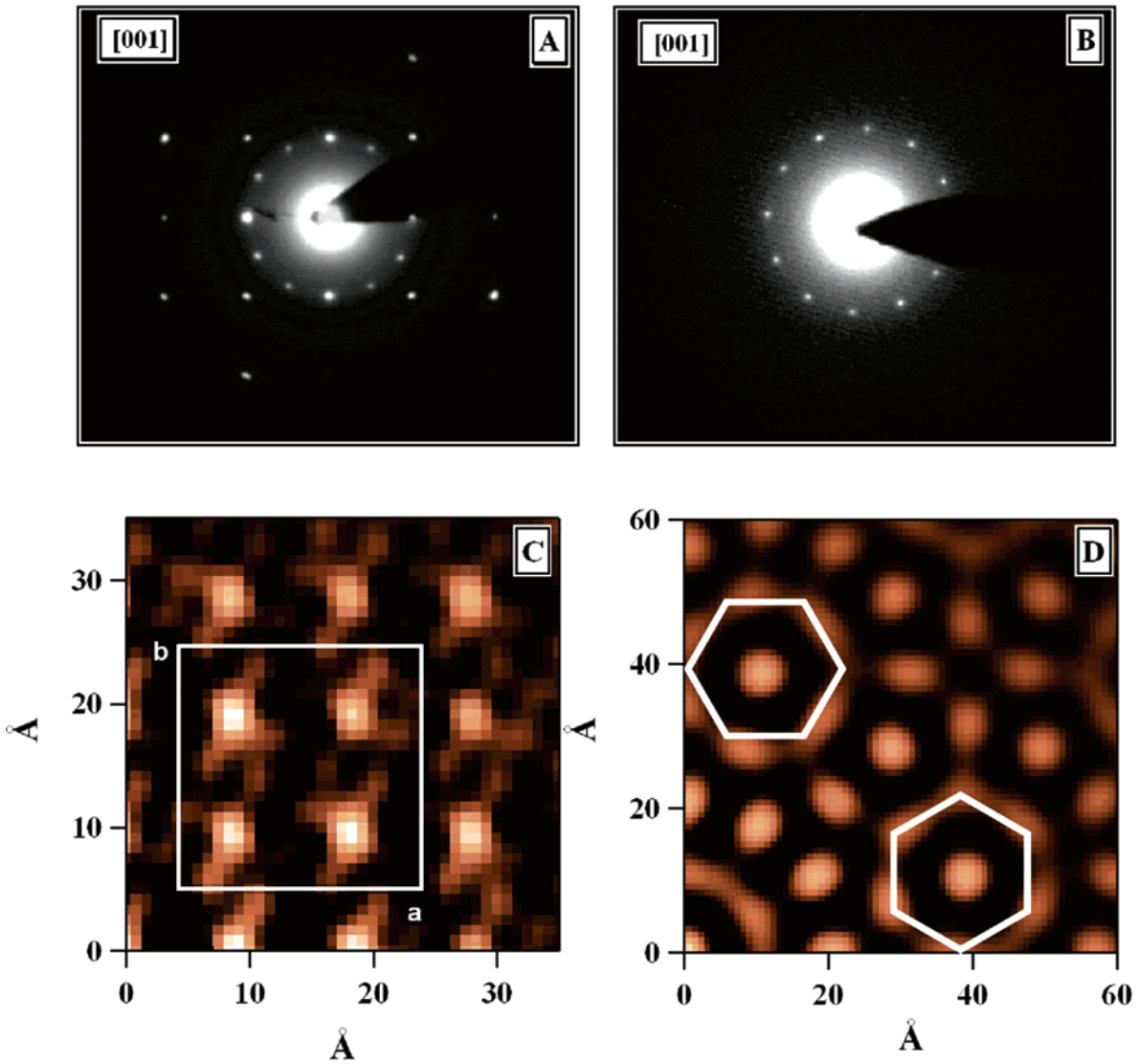

Figure 5. Electron diffraction patterns showing the transformation of the (A) pseudotetragonal α phase of PDPS into the (B) hexagonal columnar mesophase and the corresponding Patterson functions: (C) 30 × 30 and (D) 60 × 60 Å^2, respectively. The white hexagons show two mutually orthogonal orientations of the mesophase lattice. There is a clear interrelation between the orientations of the lattice parameters in the crystalline phase and the mesophase (see text for more detail).

variation of the sample. Processing and analysis of AFM images such as flattening and histogram calculation were performed using home-built routines written in Igor Pro (Wavemetrics Ltd.).

The 1D SAXS-type autocorrelation function, $\gamma(l)$, was computed from AFM images to quantify the morphological parameters of the structure. In the first step, the images were converted to the binary form using home-built object-recognition routines. Later, the 2D power spectral density function [$P_2(\underline{\mathbf{s}})$] was computed from AFM images [$h(\underline{\mathbf{r}})$] up to the critical, or Nyquist, frequency depending on the experimental sampling interval as

$$P_2(\underline{s}) \equiv \frac{1}{A}\left|\int_A h(\underline{r})\, W(\underline{r}) \exp(2\pi i \underline{s}\underline{r})\, d^2\underline{r}\right|^2 \quad (5)$$

where A denotes the image area and $W(\underline{r})$ is a window function.[26] The function $P_2(\underline{s})$ was then transformed into the one-dimensional PSD [$P_1(\underline{s})$] according to

$$P_1(s) = (2\pi s)^{-1} \int P_2(\underline{s}')\, \delta(|\underline{s}'| - s)\, d\underline{s}' \quad (6)$$

and finally, the 1D SAXS-type correlation function[27] was computed as the real part of the Fourier transform of $P_1(s)$

$$\gamma(l) \approx \mathrm{Re}[2\pi \int_0^\infty P_1(s) s \exp(2\pi i s l) \exp(4\pi^2\sigma^2 s^2)\, ds] \quad (7)$$

where the function $P_1(s)$ was preliminarily corrected for the presence of the sigmoidal gradient crystal/amorphous transition layers having thickness σ.[28] Because the absolute values of the power spectral density function of AFM images do not have any particular physical meaning (in contrast to the absolute intensity measurements in SAXS), the function $\gamma(l)$ was normalized to 1 at the origin ($l = 0$). The characteristic periodicity in the system can be determined from the position of the first subsidiary maximum of the correlation function in the self-correlation triangle.

III. Results and Discussion

III.1. Single-Crystal Morphology. Figure 1 shows typical tapping-mode AFM images of solution-grown single crystals of PDPS. It can be seen that both isolated crystals (Figure 1A) and multilayer lamellae exhibiting spiral overgrowth (Figure 1B) can be found. There is no preferential handedness of the spirals as both left- and right-handed spirals were observed in the preparation. The cross-section profiles calculated from the images (Figure 1C) indicate that the individual-crystal thicknesses are similar for the two crystals shown in images 1A and 1B and equal approximately 16 nm. The PDPS crystal shape is rectangular, with the difference between the two main dimensions being approximately 30%. This observation indirectly

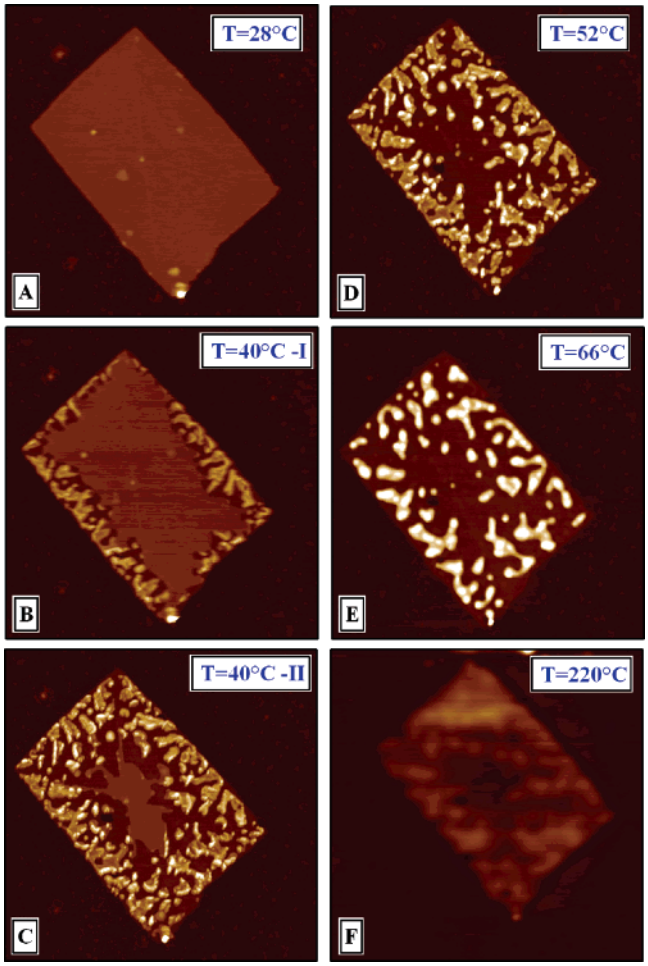

Figure 6. Topographic tapping mode AFM images (13 × 13 μm^2) showing the morphological evolution of a single crystal of PDPS as a function of temperature. The temperature program included heating steps of 1−2 °C. The images were captured after equilibration of the sample temperature for 2 min. The dwelling time of the crystal at 40 °C was approximately 1 h; the images in B and C were measured at the onset and end of the annealing at this temperature.

confirms the previous finding[9] that the crystal symmetry is lower than tetragonal. The single crystal in Figure 1A is clearly sectored: the sector boundaries run along the crystal diagonals (marked with blue arrows). It is noteworthy that the PDPS single crystals do not exhibit characteristic pleats, which are well-documented for PE single crystals.[29] These pleats, which typically form along the sector boundaries, result from the collapse of hollow pyramidal crystals of PE upon deposition on a substrate. Therefore, the absence of these features in the morphology of PDPS single crystals suggests that they might be initially flat in solution.

III.2. Selected-Area Electron Diffraction. A typical selected-area ED pattern obtained from a single crystal of PDPS is presented in Figure 2A. The inset of the figure shows the corresponding bright-field image. The PDPS crystal was oriented normal to the electron beam, but its correct in-plane orientation is not preserved in the figure [the growth faces are the (200) and (020) planes]. The ED pattern exhibits a square array of diffraction peaks, which were assigned to the (*hk*0) reciprocal space plane or the [001] zone-axis diffraction pattern. This assignment implies that the PDPS chains are oriented perpendicularly to the lamellar basal plane. The (*hk*0) diffraction peaks could be indexed to a tetragonal unit cell, but a detailed examination of the peak intensities shows that the pattern does not have 4-fold symmetry. For example, the (040) peak is significantly stronger than the (400) peak (cf. Figure 2A). These findings are in line with previous work,[9] in which a monoclinic symmetry group ($C2/c$) was proposed for the pseudotetragonal α phase of PDPS. It should be mentioned that the absence of a 4-fold symmetry in (*hk*0) patterns is at variance with previous reports.[8]

The *ab* projection of the recently proposed[9] unit cell of the α phase of PDPS is shown in Figure 2 (top). It is of interest to compare the simulated and experimental ED patterns as the unit cell refinement performed with the Rietveld method was based only on 1D diffractograms.[9] To improve the match between the experimental and simulated ED patterns, the overall isotropic temperature factor B was adjusted by minimizing the weighted-profile R factor, R_{wp}, given as

$$R_{wp} = \sqrt{\frac{\sum w_i[cI_{sim}(hkl) - I_{exp}(hkl)]^2}{\sum w_i[I_{exp}(hkl)]^2}} \qquad (8)$$

In eq 8, $w_i = 1/[I_{exp}(hkl)]$ is a weighting function; c is a scaling factor; and $I_{sim}(hkl)$ and $I_{exp}(hkl)$ are the simulated and background-corrected experimental intensity of the ED peaks, respectively. It was found that the best fit to the experimental pattern corresponds to a B value of 15.3 Å^2, and R_{wp} was found to be 0.336. The simulated ED is shown in Figure 2B. It satisfactorily reproduces the positions of the strongest diffraction peaks such as 200, 020, 240, and $4\bar{2}0$ that define the "handedness" of the pattern. A discrepancy is found for the intensity of the 400 reflection, which is more intense in the experimental than in the simulated pattern. A possible explanation for this fact is multiple scattering on the very strong 200 peak, which would significantly reinforce the faint 400 reflection.

Figure 3 shows electron diffraction patterns recorded upon progressive tilting of the crystal about the *b* axis. The patterns in Figure 3A and 3B can be assigned to the $[0\bar{1}3]$ and $[0\bar{1}2]$ zone-axis diffraction patterns, respectively. The theoretical tilt angles for these zone axes are 52.7° and 62.3°, which are in close agreement with the experimentally measured angles of 53° and 60° (maximum tilt allowed by the tilting stage). The indexing of diffraction peaks provided in the figures shows that they obey the I-centering extinction rule (hkl, $h + k + l = 2n + 1$, where n is an integer number). This result confirms the choice of symmetry group for the α phase of PDPS reported previously.[9]

Comparison of the structural model and ED experiment can be clarified by performing the analysis in direct space. The 2D Patterson function computed from the experimental (*hk*0) zonal pattern is displayed in Figure 4A. The regions with higher electron density correspond to the locations of the main chain. In addition, the position of the less-dense alkyl side chains is still clearly distinguishable in the Patterson function. It should be stressed that the information contents in the potential map and in the autocorrelation functions are principally different. In the present case, one could be confused by their similarity [cf. Figure 2 (top) and Figure 4A], which is a purely mathematical effect due to the presence of a spatially localized electron-rich backbone that can be viewed as a delta function on the potential map. The comparison of the experimental and simulated autocorrelation functions, obtained from the model, shows good agreement (Figure 4B). For example, in both cases, the lateral chains, splaying at almost right angles with respect to each other, seem to have a nearly extended conformation.

The mesomorphic character of PDPS, which has a very broad temperature window of mesophase stability, opens the possibility of studying the crystallography of this transition with good

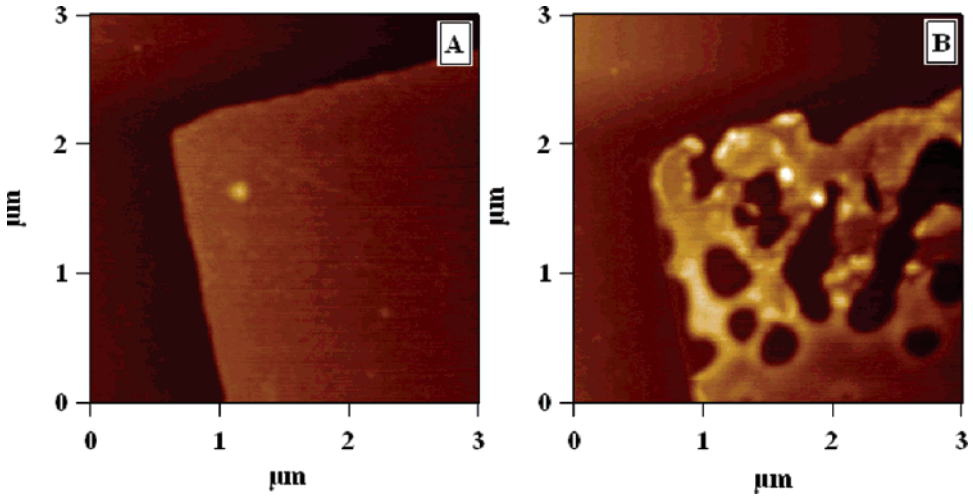

Figure 7. Small-scale ($3 \times 3\ \mu m^2$) topographic tapping mode AFM images at (A) ambient temperature and (B) 43 °C showing the initial stages of the crystal transformation. Note the typical swiss-cheese morphology with thickened regions and holes in B.

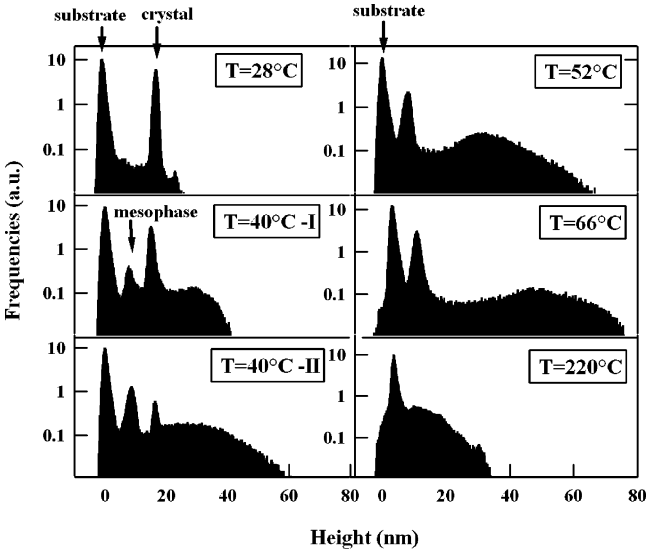

Figure 8. Height histograms obtained from the images in Figure 6 after preliminary background correction. The positions of the substrate, the initial value of the crystal thickness, and the mesomorphic regions are indicated by arrows.

spatial resolution. The transition was followed in situ in the electron microscope, where it was induced by the interaction of the sample and the electron beam. Formation of the hexagonal columnar phase is accompanied by the appearance of additional spots in the diffraction pattern (Figure 5A). These peaks, oriented at 30° with respect to the first peaks of the pseudo-tetragonal lattice, can be indexed as (100) peaks of the hexagonal lattice. At the final stage of the transformation, only the mesophase peaks are visible (Figure 5B). The fact that the mesophase pattern exhibits 12 spots indicates the presence of two hexagonal lattices oriented at 90° with respect to each other. There is a clear crystallographic interrelation between the orientation of the initial crystalline and resulting liquid crystalline (LC) lattices: the 2**a*** and 2**b*** reciprocal lattice vectors of the crystal coincide with the **a*** vectors of each of the two differently oriented hexagonal mesophases. The transition from the crystal to the mesophase occurs by sliding of the backbone axes along either the *a* or *b* axis of the crystal. To gain more insight into the mechanism of this transformation, the corresponding Patterson functions were calculated (Figure 5C,D). During the course of the transition, the lateral chains become disordered (Figure 5C). At the end of the transformation, the order of the side chains is completely lost, and the backbones do not preserve any preferential orientation, which is characteristic of the classical columnar mesophase.

III.3. Following the Melting of a PDPS Single Crystal with Atomic Force Microscopy. The melting of a 17 nm thick PDPS single crystal was followed in real time using variable-temperature tapping mode AFM. Successive images of the same crystal taken at different temperatures are displayed in Figure 6. The initial image of the crystal at ambient temperature is shown in Figure 6A. The onset of the transformation upon heating occurs at about 39 °C (image not shown here) by thickening of crystal edges, similarly to PE single crystals.[30,31] This means that the PDPS single crystal melts approximately 23 °C below the melting temperature of the bulk material, as determined by DSC (62 °C). Such a difference in the thermal stability of solution-grown and melt-crystallized material supports previous findings[9] showing that the mesophase-assisted PDPS crystallization in the bulk results in the formation of nearly extended-chain crystals.

Further heating of the crystal to 40 °C (Figure 6B) brings about the formation of numerous bright patches (thickened regions) surrounded by black zones. The vertical chain orientation in the thickened regions is likely to be preserved, as could be concluded from the ED data. The black zones separating the untransformed and transformed regions could be attributed to the LC state of the material. To assess the kinetics of the transition under isothermal conditions, the crystal was annealed at 40 °C for 1 h while continuing the image capture. One of the images recorded at the end of annealing at this temperature is shown in Figure 6C. It can be seen that the regions that started to thicken first became even thicker (brighter in the image). The transition front gradually propagates toward the center of the crystal, leaving only a small central region of the crystal intact (Figure 6C). In a parallel experiment (annealing at 40 °C for 30 min, followed by quenching to room temperature), single crystals were examined in the electron microscope. They display the superposition of tetragonal and 12-spot (double) hexagonal patterns analogous to Figure 5A (not shown). (The stability of the mesophase in thin films is further examined in section III.5.) Upon further heating of the crystal to 52 °C (Figure 6D), the central untransformed part of the crystal completely disappears. At 66 °C (Figure 6E), the crystal continues to thicken, which involves a significant material transfer. Interestingly, the thickening crystal does not fully dewet the substrate, and the

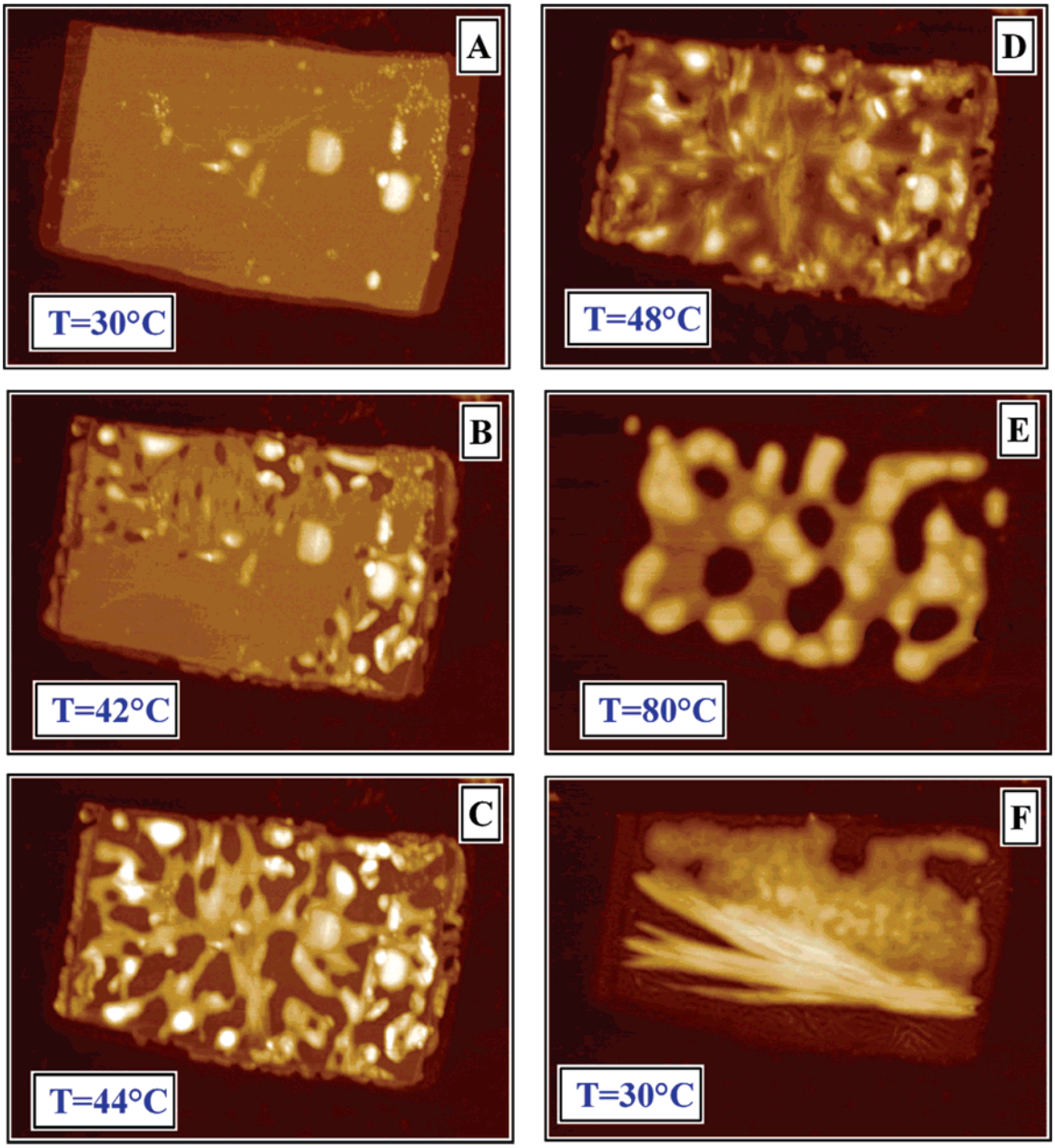

Figure 9. Successive topographic tapping mode AFM images showing the morphological evolution of a double single crystal of PDPS as a function of temperature.

initial crystal contours are still visible. Upon heating of the crystal to 220 °C, i.e., above the clearing point of PDPS, the material passes into the isotropic melt, and the crystal recovers its original shape (Figure 6F), becoming thin again. Fine morphological features appearing during thickening of the crystal can be observed in higher-magnification images taken near the crystal corner (Figure 7). The transforming crystal displays a typical "swiss-cheese" morphology with thickened regions and holes. To quantify the morphological evolution of the PDPS crystal upon heating, height histograms were computed for the images in Figure 6. The results are displayed in Figure 8. The peaks corresponding to the Si substrate and to the initial crystal thickness are indicated by arrows. Upon heating, the intensity of the peak at 17 nm decreases, and a new peak appears at 8 nm and grows. This process is accompanied by the formation of a broad maximum corresponding to the thickened regions, the thickness of which extends to 60−80 nm. The peak at 8 nm corresponds to the height of the black zones mentioned previously. These regions are likely to be mesomorphic and, at some stage of the crystal evolution, separate the transformed and intact areas (cf. Figure 6B,C). Therefore, the formation of the mesophase precedes the crystal thickening and is followed by a re-entrant transition to the crystalline state, similar to the one described for PBD.[7] This result indicates that the evolution of PDPS single crystals can occur via a short-term dwelling in the mesophase, where the chains acquire a significant mobility. This mobility can also account for the exceptional range of accessible crystal thickness of PDPS, which is much larger than that observed for PE single crystals.[3]

III.4. Melting of a Superposition of Two PDPS Single Crystals. The thermal behavior of superposed single crystals can significantly differ from the behavior of individual crystals, as the former have additional possibilities for chain motion. Topographic tapping mode AFM images recorded from a double PDPS crystal at different temperatures are shown in Figure 9.

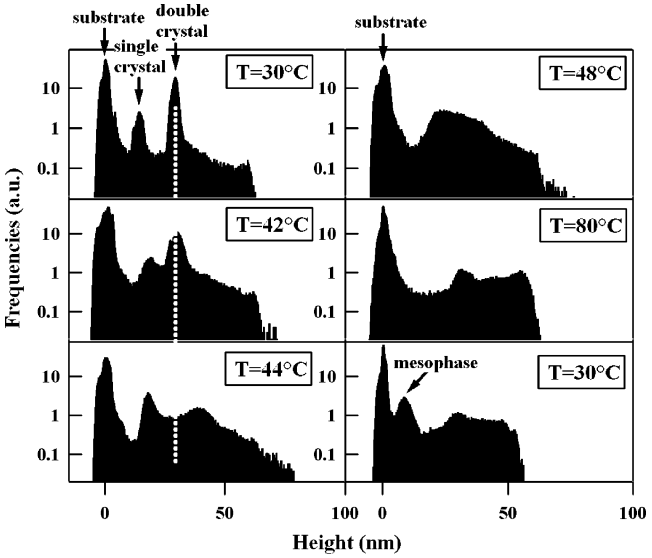

Figure 10. Height histograms obtained from the images in Figure 9 after background correction. The positions of the substrate, superposed crystal, and mesomorphic regions are indicated.

The initial image at ambient temperature (Figure 9A) shows that the bottom crystal is slightly larger that the top one. The bright spots visible on the surface of the crystal are probably aggregates of noncrystallized material precipitated from solution. The characteristic heights of the crystals can be seen in the height histogram presented in Figure 10. Three stages can be clearly distinguished in the melting process of the double crystal. In the first stage, the top crystal starts thickening and dewets the underlying crystal. The onset of the process occurs at a slightly higher temperature than in the previous experiment (Figure 9B). However, the way the chains reorganize in the top crystal might be rather different from the case of a single crystal discussed earlier. Indeed, the morphological features seen in a higher-magnification image in Figure 11, corresponding to the upper left corner of the crystal in Figure 9B, indicate that, at 42 °C, the chain orientation in the top crystal is likely to be in the plane of the substrate. In this case, regular stripes, similar to the ones present in layers of ultralong alkanes,[3] are observed. The periodicity (long period) of the structure is approximately 60 nm, as can be seen from the position of the first subsidiary maximum in $\gamma(l)$ (Figure 11, bottom). The linear crystallinity, defined as the ratio of the crystal thickness to the long period, is estimated to be 71%. This indicates that the thickness of the PDPS crystal increases many times compared to its initial value. However, at this low temperature, the crystal thickness is still far from the contour length of the PDPS chain (163 nm). At 44 °C, the top crystal is completely transformed (cf. Figures 9C and 10). The second stage starts at about 45 °C with the beginning of transformation of the bottom crystal (Figure 9D). One can notice that the clear double-layer structure is no longer present, which suggests that the chains can now slide between the crystals. This high chain mobility giving rise to merging of the superposed PDPS crystals is different from the behavior of superposed PE crystals that are reported to thicken independently.[31] In the third stage, upon a further temperature increase, the two crystals continue to thicken as one object (Figure 9E), reaching the thickness value of about 60 nm at 80 °C. After being heated in the isotropic phase, the crystal thins by recovering its original shape, similar to the observation reported in the previous section. Upon cooling of the molten material to ambient temperature, the crystal forms again, displaying a different morphology characterized by elongated ribbons (Figure

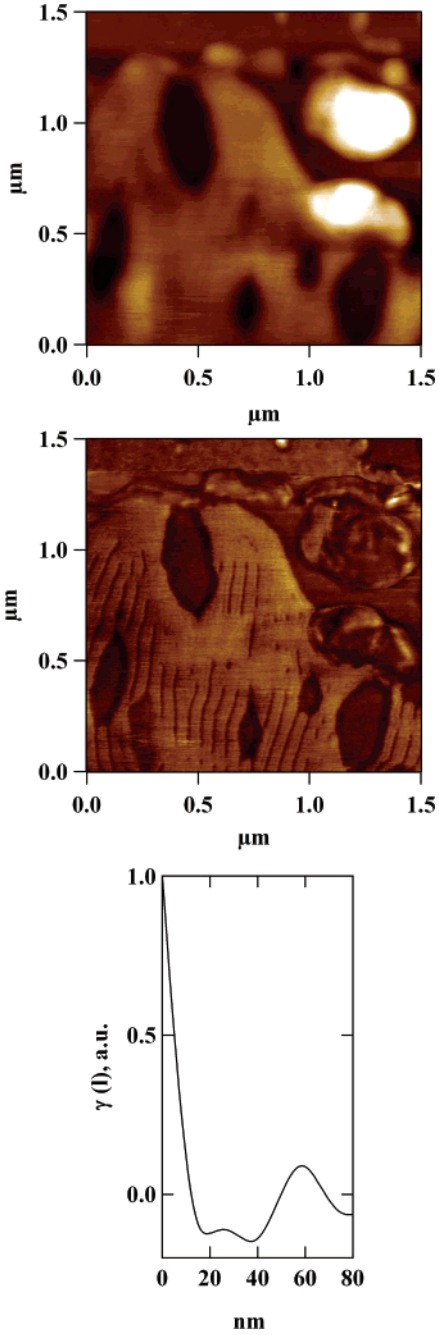

Figure 11. Tapping mode (top) height and (middle) phase AFM images measured on the transformed double crystal of PDPS shown in Figure 6F. The image exhibits a striped morphology similar to the layers of ultralong *n*-alkanes.[3] (bottom) The SAXS-type autocorrelation function corresponding to the phase image shows that the characteristic stripe thickness is approximately 60 nm.

9F). The corresponding histogram displays a peak situated at approximately 30 nm that correspond to the crystal thickness and a second peak at 8 nm that can be assigned to the mesomorphic material, similar to what was observed for the reorganization of a single crystal (cf. section III.3).

III.5. Transforming a PDPS Single Crystal at Ambient Temperature with the AFM Tip. It is well-documented that, in contrast to other members of the family of poly(di-*n*-alkylsiloxanes), bulk PDPS cannot be obtained in an amorphous or mesomorphous state at ambient temperature because of its high crystallization rate.[10] Recently, it was suggested that PDPS could retain its LC character at ambient temperature when confined in thin layers.[9] This behavior was explored in more

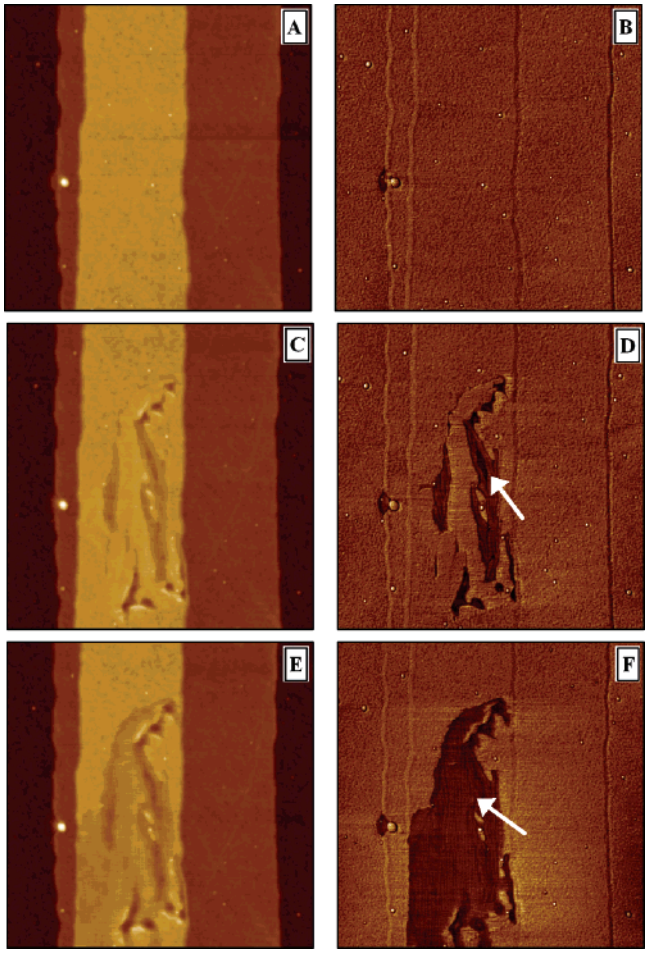

Figure 12. Tapping mode (A,C,E) topography and (B,D,F) phase images illustrating the morphological evolution of a single PDPS crystal induced by the tip−sample interaction at ambient temperature. The initial double-layer crystal is shown in A and B. It was probably folded and broken at the moment of its deposition on the surface. Upon repetitive imaging of the crystal with an increased tapping force (C−F), growth of topographical defects (marked by blue arrows) appears. These regions, which probably have mesomorphic character, exhibit organization in ribbons oriented parallel to the scanning direction.

detail in the present work for the case of PDPS single crystals. Figure 12 shows tapping mode height and phase images of a single PDPS crystal at ambient temperature. Upon repeated scanning of the same region with an increased tapping force, growth of topographical defects appears. These defects are dark in the phase images and display a ribbonlike structure, with the ribbons parallel to the scanning direction. The contrast observed in the phase images can be explained by the LC state of the ribbons, which are softer than the crystal. The orientation of the ribbons could indicate that the PDPS chains become aligned by the scanning tip. Thus, the mesomorphic regions, which can be generated by the AFM tip inducing local melting of the PDPS single crystal, remain stable at ambient temperature because of the conditions of confinement.

Conclusions

Crystallization of PDPS from a dilute solution results in the formation of thin chain-folded lamellae having a rectangular shape. Both individual and multilayer crystals exhibiting spiral overgrowths were observed. Examination of different zonal electron diffraction patterns measured on single crystals supports the choice of a monoclinic symmetry space group for the α phase of PDPS that was proposed previously.[9] The unit-cell structure of the α phase of PDPS established on the basis of the Rietveld refinement of 1D X-ray diffraction data[9] was checked by comparing the experimental and simulated electron diffraction intensities and the Patterson functions. A reasonably good agreement was found for the positions of the most intense diffraction peaks determining the handedness of the [001] zone-axis diffraction pattern. The conformation of the lateral side chains was found similar in the simulated and experimental Patterson functions corresponding to this zone axis.

The crystal-to-columnar mesophase transition was studied in situ with selected-area electron diffraction. It was observed that the mesophase displays two mutually orthogonal orientations of the lattice. The orientations of the 2**a*** and 2**b*** reciprocal lattice vectors of the crystal coincide with the **a*** vectors of each of the two differently oriented mesophases. The in situ AFM study of the evolution of a single PDPS crystal upon heating shows that crystal thickening can occur via a short-term dwelling in the mesophase. This high chain mobility in the mesophase can account for the exceptional range of accessible crystal thicknesses of PDPS, which is much larger than that observed for PE single crystals.

Acknowledgment. This work was financially supported by the RFBR (Grant 02-03-32199), INTAS (Grant 00-525), and Communauté Française de Belgique (ARC No. 00/05-257). We are grateful to M. H. J. Koch (EMBL, Hamburg, Germany) for reading this manuscript and providing fruitful comments.

References and Notes

(1) Keller, A. *Philos. Mag*. **1957**, *2*, 1171.
(2) Ungar, G.; Zeng, X. *Chem. Rev.* **2001**, *101*, 4157.
(3) Magonov, S. N.; Yerina, N. A.; Ungar G.; Reneker D. H.; Ivanov, D. A. *Macromolecules* **2003**, *36*, 5637.
(4) Matsuda, H.; Aoike, T.; Uehara, H.; Yamanobe, T.; Komoto, T. *Polymer* **2001**, *42*, 5013.
(5) Sirota, E. B.; King, H. E.; Hughes, G. J.; Wan, W. K. *Phys. Rev. Lett.* **1992**, *68*, 492.
(6) Hocquet, S.; Dosière, M.; Thierry, A.; Lotz, B.; Dubreuil, N.; Koch, M. H. J.; Ivanov, D. A. *Macromolecules* **2003**, *36*, 8376.
(7) Rastogi, S.; Ungar, G. *Macromolecules* **1992**, *25*, 1445.
(8) Petersen, D. R.; Carter, D. R.; Lee, C. L. *J. Macromol. Sci.−Phys.* **1969**, *B3* (3), 519.
(9) Gearba, R. I.; Anokhin, D. V.; Bondar, A. I.; Godovsky, Yu. K.; Papkov, V. S.; Makarova, N. N.; Magonov, S. N.; Bras, W.; Koch, M. H. J.; Masin, F.; Goderis, B.; Ivanov, D. A. *Macromolecules*, **2006**, *39*, 988.
(10) Godovsky, Yu. K.; Makarova, N. N.; Papkov V. S.; Kuzmin, N. N. *Makromol. Chem., Rapid Commun*. **1985**, *6*, 443.
(11) Godovsky Yu. K.; Mamaeva, I. V.; Makarova, N. N.; Papkov, V. S.; Kuzmin, N. N. *Makromol. Chem., Rapid Commun*. **1985**, *6*, 797.
(12) Shulgin A. I.; Godovsky, Yu. K. *Polym. Sci. USSR* **1987**, *29*, 2845.
(13) Godovksy, Yu. K.; Papkov, V. S. *Makromol. Chem., Macromol. Symp*. **1986**, *4*, 71.
(14) Shulgin, A. I.; Godovsky, Yu. K.; Makarova, N. N. *Thermochim. Acta* **1994**, *238*, 337.
(15) Out, G.; Turetskii, A.; Moeller, M. *Makromol. Chem., Rapid Commun*. **1995**, *16*, 107.
(16) Out, G.; Siffrin, S.; Frey, H.; Oelfin, D.; Koegler, G.; Moeller, M. *Polym. Adv. Technol.* **1994**, *5*, 796.
(17) Godovsky, Yu. K.; Papkov, V. S.; Magonov, S. N. *Macromolecules* **2001**, *34*, 976.
(18) Molenberg, A.; Moeller, M.; Sautter, E. *Prog. Polym. Sci.* **1997**, *22*, 1133.
(19) Ungar, G. *Polymer* **1993**, *34*, 2050.
(20) Bassett, D. C.; Khalifa, B. A.; Turner, B. *Nat. Phys. Sci*. **1972**, *239*, 106.
(21) Bassett, D. C.; Turner, B. *Nat. Phys. Sci*. **1972**, *240*, 146.
(22) Mott, N.; Massey, H. *The Theory of Atomic Collisions*; Clarendon Press: Oxford, U.K., 1965.
(23) *International Tables for Crystallography*, 1st ed.; Kluwer Academic Publishers: Dordrecht, The Netherlands, 2002; Vol. B.
(24) Ivanov, D. A.; Daniels, R.; Magonov, S. Exploring the High-Temperature AFM and Its Use for Studies of Polymers. Application note published by Digital Instruments/Veeco Metrology Group, 2001,

pp 1−12. Available online at http://www.veeco.com/appnotes/AN45_HighTempHeater_090104_RevA1.pdf.
(25) Ivanov, D. A.; Amalou, Z.; Magonov, S. N. *Macromolecues* **2001**, *34*, 8944.
(26) Press, W. H.; Flanerry, B. P.; Teukolsky, S. A.; Vetterling, W. T. *Numerical Recipes in C: The Art of Scientific Computing*, 1st ed.; Cambridge University Press: New York, 1988.
(27) Ruland, W. *Colloid Polym. Sci*. **1977**, *255*, 417.
(28) Koberstein, J. T.; Morra, B.; Stein, R. S. *J. Appl. Crystallogr*. **1980**, *13*, 34.
(29) Bassett, D. C.; Frank, F. C.; Keller, A. *Philos. Mag.* **1963**, 1739.
(30) Hobbs, J. K.; Hill, M. J.; Barham, P. J. *Polymer* **2000**, *41*, 8761.
(31) Organ, S. J.; Hobbs, J. K.; Miles, M. J. *Macromolecules* **2004**, *37*, 4562.

MA051606G